Received September 1999
Revised September 2001
Accepted October 2001

Numerical simulation of forced convection flow past a parabolic cylinder embedded in porous media

O.M. Haddad, M.A. Al-Nimr and M.A. Abu-Ayyad
Department of Mechanical Engineering, Jordan University of Science and Technology, Irbid, Jordan

Keywords *Numerical simulation, Finite differences, Forced convection, Porous media*

Abstract *Numerical solutions are presented for steady two-dimensional symmetric flow past a parabolic cylinder embedded in porous media. For this study, the full Navier–Stokes equations (combined with the Brinkman–Forchheimer-extended Darcy model) and energy equation in parabolic coordinates were solved. A second order accurate finite difference scheme on a non-uniform grid was used. A wide range of Reynolds number (Re) is studied for different values of Prandtl number (Pr). It is found that the pressure, skin friction and Nusselt number decreases as the Darcy number (Da) decreases and/or the Inertia parameter (Λ) increases.*

Nomenclature

C_f = Skin friction coefficient ($\tau_w/\rho U_\infty^2$)
Cp_f = Specific heat of the fluid
D = Reference length
Da = Modified Darcy number ($\rho U_\infty^2 K_p/\nu_f{}^2$)
F = Empirical constant in the second-order resistance
f = Modified stream function (ψ/ζ)
g = Modified vorticity ($-(\zeta^2+\eta^2)\omega/\zeta$)
h = Modified temperature ($-(\zeta^2+\eta^2)\theta/\zeta$)
ho = Heat transfer coefficient
k = Thermal conductivity
K = Permeability
kr = The conductivity ratio (k_e/k_f)
Nu = Nusselt number ($h_o D/k_f$)
p^* = Dimensional local pressure
p = Non-dimensional local pressure ($(p^* - p_\infty)/\rho U_\infty^2$)
P = Modified non-dimensional local pressure ($p - (\eta/(\zeta^2+\eta^2))g(0,\mathrm{Re}^{1/2})$)
Pr = Prandtl number (ν_f/α_f)
Pr_e = Effective Prandtl number (ν_f/α_e)
R = Nose radius of curvature
Re = Reynolds number based on the nose radius of curvature (RU_∞/ν_f)
T = Temperature
U_∞ = Free-stream velocity
(u,v) = Velocity component in (x,y) directions, respectively
(x,y) = Cartesian coordinates
$X_{\max}$ = The surface maximum non-dimensional x – coordinate value ($x_{\max}/(\nu_f/U_\infty)$)
VR = Viscosity ratio (ν_e/ν_f)

Greek symbols

α = Thermal diffusivity
ϵ = Porosity
Λ = Inertia parameter ($F_p\epsilon/K_p{}^{1/2}$)
$\bar{\Lambda}$ = Modified inertia parameter ($\nu_f\Lambda/U_\infty$)
ν = Kinematic viscosity
θ = Non-dimensional temperature ($(T - T_\infty)/(T_w - T_\infty)$)
ρ = Fluid density
τ_w = Shear stress at the wall ($\mu(\partial u/\partial y)_w$)
ψ = Stream function
ω = Vorticity

International Journal of Numerical Methods for Heat & Fluid Flow, Vol. 12 No. 1, 2002, pp. 6–28.

DOI 10.1108/09615530210413145

ΔT = Temperature difference ($T_w - T_\infty$)
(ζ,η) = The parabolic coordinates

Subscripts

e = effective
f = fluid
p = porous
s = solid matrix of the porous material
w = wall condition
∞ = free-stream condition

Introduction

The problem of flow over parabolic bodies is of importance in properly determining the local solutions near leading edges in more complicated problems. Those who study numerical solutions of the Navier–Stokes equations of such flows usually ignore the singularities that exist at the leading edge. One of the earliest analyses was presented by Van Dyke (1962) who considered that there is no singularity at the nose of the parabolic body, as in the case of the semi-infinite flat plate. On the parabolic body, the flow proceeds without separation from stagnation point flow at the nose to Blasius flow farther downstream. Dennis and Walsh (1971) obtained numerical solution for the steady symmetric viscous flow past a parabolic cylinder in a uniform stream. They obtained a solution using two-dimensional finite-difference approximations to the partial differential equations for the stream function and vorticity. Their solutions cover the range of Reynolds number (based on the nose radius of the cylinder) from 0.25 to ∞. Davis (1972) obtained a numerical solution of the Navier–Stokes equations for symmetric laminar incompressible flow past a parabola. The governing equations were solved numerically using an Alternating Direction Implicit (ADI) method. To remove the singularity from the problem in the limit as Reynolds number goes to zero, Davis introduced a set of dependent and independent variables, which seem ideally suited to the problem.

Haddad and Corke (1998) have numerically studied the effect of curvature of the leading edge on the boundary-layer receptivity of a two-dimensional laminar incompressible flow over parabolic bodies. Haddad *et al.* (2000) presented a numerical solution of Navier–Stokes and energy equations for laminar, steady and two-dimensional symmetric flow past a parabolic cylinder in a uniform stream parallel to its axis. The full Navier–Stokes equations and energy equation in parabolic coordinates were solved using finite difference technique. A wide rang of Reynolds numbers is studied for different values of Prandtl number.

The problem of forced convection heat transfer over a flat plate embedded in a medium totally or partially filled with porous material is investigated by Vafai and Tien (1981), Vafai (1984), Kaviany (1987), Vafai and Kim (1990) and Huang and Vafai (1994). However, these studies presented solutions for the approximate boundary layer governing equations, which are valid for locations far away from the leading edge.

The objective of the present work is to study the effect of the presence of an-isotropic solid matrix on the hydrodynamic and heat transfer (forced convection) characteristics of the flow over a parabolic body using the finite difference technique. The leading-edge region was not excluded but rather was part of the solution domain. Using parabolic coordinates, the natural extension of the flat plate to other body shapes is the parabolic cylinder, which is the focus of the present investigation. The formulation allows the flat plate solution to arise as a special case when Reynolds number based on the nose radius of curvature equals to zero.

Formulation of the problem

Governing equations

Figure 1 shows a schematic diagram for the physical problem under consideration. It is assumed that the flow is steady, two-dimensional, laminar and incompressible. The parabolic-body is surrounded by a porous medium, as shown in the figure. The equation of the surface of the parabolic-body is given by

$$x(y) = \frac{1}{2R}(y^2 - R^2) \tag{1}$$

where R is recognized as the nose radius of curvature.

The conservation equations (in dimensional form) of the flow in a porous medium are based on a general flow model. This generalized flow model is also known as the Brinkman–Forchheimer-extended Darcy model (Vafai and Tien, 1981; Kaviany, 1995):

$$\frac{\partial u}{\partial x} + \frac{\partial v}{\partial y} = 0 \tag{2}$$

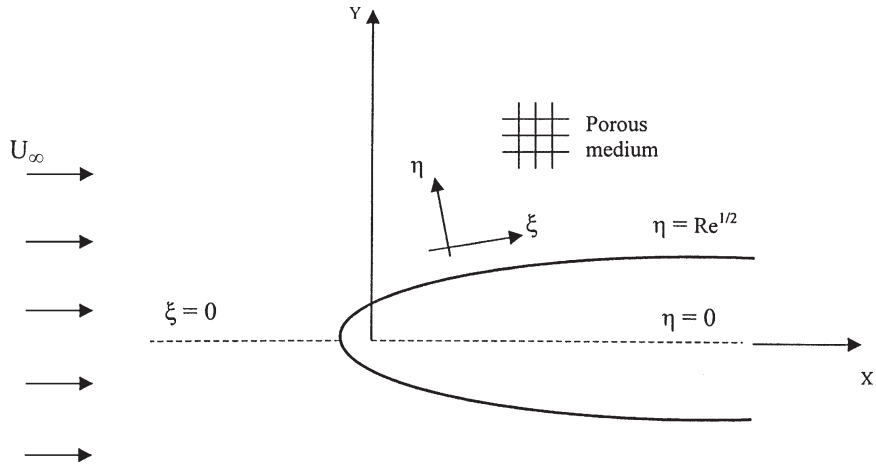

Figure 1.
Schematic diagram

$$u\frac{\partial u}{\partial x}+v\frac{\partial u}{\partial y}=-\frac{1}{\rho_f}\frac{\partial p}{\partial x}-\frac{\nu_f}{K_p}u-\Lambda u\sqrt{u^2+v^2}+\nu_e\left(\frac{\partial^2 u}{\partial x^2}+\frac{\partial^2 u}{\partial y^2}\right) \quad (3)$$

$$u\frac{\partial v}{\partial x}+v\frac{\partial v}{\partial y}=-\frac{1}{\rho_f}\frac{\partial p}{\partial y}-\frac{\nu_f}{K_p}v-\Lambda v\sqrt{u^2+v^2}+\nu_e\left(\frac{\partial^2 v}{\partial x^2}+\frac{\partial^2 v}{\partial y^2}\right) \quad (4)$$

$$u\frac{\partial T}{\partial x}+v\frac{\partial T}{\partial y}=\alpha_e\left(\frac{\partial^2 T}{\partial x^2}+\frac{\partial^2 T}{\partial y^2}\right) \quad (5)$$

where Λ is the inertia parameter

$$\Lambda=\frac{F_p\varepsilon}{\sqrt{K_p}} \quad (6)$$

and

$$\sqrt{u^2+v^2}\cong u \quad \text{if} \quad u\gg v$$

Also α_e is defined as

$$\alpha_e=k_e/\varepsilon\rho_f Cp_f, \quad k_e=k_s(1-\varepsilon)+\varepsilon k_f \quad (7)$$

where k_f, ρ_f and Cp_f refer to the thermal conductivity, density and heat capacity of the fluid, respectively.

Equations (2)–(5) are obtained by Vafai and Tien (1981) using the local volume averaging and matched asymptotic expansion techniques under the assumption of two-dimensional, steady, isotropic, incompressible and homogeneous flow through a fluid-saturated porous medium.

It has been found that setting the effective viscosity (ν_e) of the fluid-saturated porous medium equal to the viscosity of the fluid provides good agreement with experimental data (Lundgern, 1972; Neale and Nader, 1974). This approximation is adopted in the present work.

Introducing the stream function (ψ) and the vorticity (ω) such that

$$u=\frac{\partial \psi}{\partial y}, \quad v=\frac{\partial \psi}{\partial x}, \quad \omega=\frac{\partial v}{\partial x}-\frac{\partial u}{\partial y} \quad (8)$$

the stream-function, vorticity and energy equations in terms of ψ, ω and T are then in the form:

$$\frac{\partial^2 \psi}{\partial x^2}+\frac{\partial^2 \psi}{\partial y^2}=-\omega \quad (9)$$

$$\nu_e\left(\frac{\partial^2\omega}{\partial x^2}+\frac{\partial^2\omega}{\partial y^2}\right)+\frac{\partial\psi}{\partial x}\frac{\partial\omega}{\partial y}-\frac{\partial\psi}{\partial y}\frac{\partial\omega}{\partial x}$$

$$=\left(\frac{\nu_f}{K_p}+\Lambda\frac{\partial\psi}{\partial x}\right)\omega-\Lambda\left(\frac{\partial\psi}{\partial y}\frac{\partial^2\psi}{\partial y^2}+\frac{\partial\psi}{\partial x}\frac{\partial^2\psi}{\partial x\partial y}\right) \tag{10}$$

$$\alpha_e\left(\frac{\partial^2 T}{\partial x^2}+\frac{\partial^2 T}{\partial y^2}\right)+\frac{\partial\psi}{\partial x}\frac{\partial T}{\partial y}-\frac{\partial\psi}{\partial y}\frac{\partial T}{\partial x}=0 \tag{11}$$

In order to convert the above equations into a non-dimensional form, the following dimensionless variable are introduced. (For convenience, the superscript (*) is used only in the definitions of the non-dimensional variables to indicate dimensional quantities.)

$$x=\frac{x*}{(\nu_f/U_\infty)},\quad y=\frac{y*}{(\nu_f/U_\infty)},\quad \psi=\frac{\psi*}{\nu_f},\quad \omega=\frac{\omega*}{\left(U_\infty^2/\nu_f\right)},$$
$$\theta=\frac{T*-T_\infty}{T_w-T_\infty} \tag{12}$$

The non-dimensional form of the governing equations is then

$$\psi_{xx}+\psi_{yy}=-\omega \tag{13}$$

$$\frac{\nu_e}{v_f}(\omega_{xx}+\omega_{yy})+\psi_x\omega_y-\psi_y\omega_x=\left(\frac{1}{\mathrm{Da}}+\bar{\Lambda}\psi_y\right)\omega-\bar{\Lambda}(\psi_y\psi_{yy}+\psi_x\psi_{xy}) \tag{14}$$

$$\frac{1}{\mathrm{Pr}}(\theta_{xx}+\theta_{yy})+\psi_x\theta_y-\psi_y\theta_x=0 \tag{15}$$

$$\mathrm{Da}=\frac{U_\infty^2 K_p}{\nu_f^2},\quad \bar{\Lambda}=\frac{\nu_f\Lambda}{U_\infty},\quad \mathrm{Pr}_e=\frac{\nu_f}{\alpha_e} \tag{16}$$

In order to transform the above equations from cartesian variables (x,y) to parabolic variables (ζ,η), the relation between the two coordinate systems is required. The non-dimensional independent variables ζ and η (parabolic

coordinates) are related to the non-dimensional x and y (Cartesian coordinates) by

$$x + iy = \frac{(\zeta + i\eta)^2}{2} \tag{17}$$

where i here is $\sqrt{-1}$.

In order to remove the singularity at the leading-edge of the flat plate case, we follow Davis (1972) and introduce the new variables f, g and h which are related to ψ, ω and θ by

$$\psi = \zeta f(\zeta, \eta), \quad \omega = -\frac{\zeta}{(\zeta^2 + \eta^2)} g(\zeta, \eta), \quad \theta = -\frac{\zeta}{(\zeta^2 + \eta^2)} h(\zeta, \eta) \tag{18}$$

(The Stokes solution near the nose of a parabola shows that $\Psi = A\zeta(\eta - R^{1/2})^2$, where A is an undetermined constant. From this expression the vorticity ω is found to be $-2A\zeta/(\zeta^2+\eta^2)$.)

The new dependent variables are then governed by the following equations

$$f_{\eta\eta} - g + f_{\zeta\zeta} + \frac{2}{\zeta} f_\zeta = 0 \tag{19}$$

$$\begin{aligned}
&\frac{\nu_e}{\nu_f} g_{\eta\eta} + \left[f + \zeta f_\zeta - \frac{4\eta}{\zeta^2 + \eta^2} \frac{\nu_e}{\nu_f} \right] g_\eta \\
&+ \left[\frac{\zeta^2 - \eta^2}{\zeta^2 + \eta^2} f_\eta - \frac{2\eta}{\zeta^2 + \eta^2} (f + \zeta f_\zeta) \right] g - \zeta \left[f_\eta + \frac{4}{\zeta^2 + \eta^2} \frac{\nu_e}{\nu_f} \right] g_\zeta \\
&- \frac{(\zeta^2 + \eta^2)}{\mathrm{Da}} g - \bar{\Lambda}[\eta(f + \zeta f_\zeta) + \zeta^2 f_\eta] g \\
&- \bar{\Lambda}\zeta(f + \zeta f_\zeta + \eta f_\eta) f_{\zeta\eta} \\
&- \bar{\Lambda} \left[\frac{2\eta}{\zeta^2 + \eta^2} \left(\eta^2 f_\zeta^2 - f^2 \right) + \zeta^2 f_\eta f_{\eta\eta} \right. \\
&\left. + \left(f + \zeta f_\zeta - \eta \left(\frac{\zeta^2 - \eta^2}{\zeta^2 + \eta^2} \right) f_\eta \right) f_\eta - \frac{4\zeta\eta}{\zeta^2 + \eta^2} f f_\zeta \right] \\
&- \bar{\Lambda} \left[\eta(f + \zeta f_\zeta) f_{\zeta\zeta} + \frac{2\eta}{\zeta} f f_\zeta \right] + \frac{\nu_e}{\nu_f} \left(g_{\zeta\zeta} + \frac{2}{\zeta} g_\zeta \right) = 0
\end{aligned} \tag{20}$$

$$h_{\eta\eta} + \left[(f + \zeta f_\zeta)\mathrm{Pr}_e - \frac{4\eta}{\zeta^2 + \eta^2}\right] h_\eta + \left[\frac{\zeta^2 - \eta^2}{\zeta^2 + \eta^2} f_\eta - \frac{2\eta}{\zeta^2 + \eta^2}(f + \zeta f_\zeta)\right] \mathrm{Pr}_e h - \zeta\left[\mathrm{Pr}_e f_\eta + \frac{4}{\zeta^2 + \eta^2}\right] h_\zeta + h_{\zeta\zeta} + \frac{2}{\zeta} h_\zeta = 0 \tag{21}$$

this system of partial differential equations is non-linear and elliptic. We also note that these equations are parabolic in ζ when the last two terms of each equation are neglected. Davis (1972) had exploited this fact to formulate an efficient numerical solution for the problem.

Boundary conditions

At the wall: $u = 0$, $v = 0$, also the vorticity at the wall is unknown and is determined by applying the stream function equation at the wall, whereas $\theta = 1$. These conditions give

$$\text{at} \quad \eta = \mathrm{Re}^{1/2}: \quad f = 0, \quad f_\eta = 0, \quad g = f_{\eta\eta} \quad \text{and} \quad h = -(\zeta^2 + \eta^2)/\zeta \tag{22}$$

At freestream: uniform flow with zero vorticity and $\theta = 0$. That is

$$\text{as} \quad \eta \to \infty: \quad f_\eta \to 1, \quad g \to 0 \quad \text{and} \quad h \to 0 \tag{23}$$

In order to evaluate the pressure along the body surface, the x − momentum equation was applied at the wall. The result in parabolic variables (ζ, η) is

$$\frac{\partial p}{\partial \zeta} = -\frac{\nu_e}{\nu_f}\frac{\partial \omega}{\partial \eta} \tag{24}$$

$$\frac{\partial p}{\partial \zeta} = -\frac{\nu_e}{\nu_f}\frac{\zeta}{(\zeta^2 + \eta^2)}\left[\frac{\partial g}{\partial \eta} - \frac{2\eta}{(\zeta^2 + \eta^2)} g\right] \tag{25}$$

To remove the singularity of the pressure at the leading edge of the flat plate, we follow Davis (1972) and introduce the following transformation. (The Stokes solution near the nose of a parabola shows that the pressure (non-dimensionalized by ρU_∞^2 is found to be $2A\eta/(\zeta 2 + \eta^2) + C$.)

$$P = p - \frac{\eta}{(\zeta^2 + \eta^2)} g\left(0, \mathrm{Re}^{1/2}\right) \tag{26}$$

thus,

$$\frac{\partial P}{\partial \zeta} = \frac{\nu_e}{\nu_f} \frac{\zeta}{\left(\zeta^2 + \eta^2\right)} \left[\frac{\partial g}{\partial \eta} - \frac{2\eta}{\left(\zeta^2 + \eta^2\right)} (g - g_o) \right] \tag{27}$$

where $g_o = g(0, \mathrm{Re}^{1/2})$. As opposed to (p), the function (P) behaves properly near $\zeta = 0$ (Davis, 1972).

The local skin friction is defined as

$$C_f = \frac{\tau_w}{\rho U_\infty^2} = -\omega|_w \tag{28}$$

$$C_f = \frac{\zeta}{\left(\zeta^2 + \eta^2\right)} g\left(\zeta, \mathrm{Re}^{1/2}\right) \tag{29}$$

The local Nusselt number is defined as

$$\mathrm{Nu} = \frac{h_o D}{k_f} \tag{30}$$

where (h_o) is the convective heat transfer coefficient, which is defined as

$$h_o = -\frac{k_e}{\Delta T} \frac{\partial T}{\partial y}\bigg|_w \tag{31}$$

and (D) is a dimensional reference length which can be equal in magnitude to $\zeta_{\max}$. Also, it should be noted that the conductivity of the fluid appears explicitly in the definition the Nusselt number, that is

$$\mathrm{Nu} = -\zeta_{\max} \frac{k_e}{k_f} \frac{\partial \theta}{\partial y}\bigg|_w \tag{32}$$

Transforming the above equation into parabolic coordinates using equation (17), then

$$\mathrm{Nu}(\zeta) = \frac{k_e}{k_f} \zeta_{\max} \left[\frac{\zeta}{\left(\zeta^2 + \eta^2\right)^2} \left[\zeta h_\eta + \eta_w h_\zeta \right] - \frac{\eta_w \left(3\zeta^2 - \eta_w^2\right)}{\left(\zeta^2 + \eta^2\right)^3} h \right] \tag{33}$$

Numerical method of solution

For the present study, we use the finite difference technique to convert the governing non-linear partial differential equations into a system of linear

algebraic equations, as follows: using finite difference approximations (FDAs), the governing non-linear partial differential equations (PDEs) are converted into non-linear finite difference equations (FDEs). The finite difference scheme is explained later in this section. The resulting non-linear FDEs are linearized using Newton's Linearization technique. As the unknown variables f, g and h appeared in the coefficients matrix, iteration was required to solve the resulting equations. The linear system is solved simultaneously by iteration using "LINPACK " subroutines (Dongarra *et al.*, 1979). At each iteration, the solution was found by solving the resulting system of linear algebraic equations simultaneously. Defining the absolute difference in the solution between the new $(n+1)$ and old (n) iterations as the "error" at iteration (n), then convergence was determined to occur when the maximum local error in f, g and h over all the domain is $< 10^{-5}$. As opposed to the numerical ADI-technique used by Davis (1972), the technique used for this study is simple, however, it requires large RAM computer facility. Therefore, this change in approach is a trade-off between computing memory requirement and speed.

In order to start the numerical code and generate the physical and numerical grids, $X_{\max}$ in the physical plane and $\eta_{\max}$ in the numerical plane must be supplied. Based on the study made by Haddad and Corke (1998) and on the capacity of the computer available for this study, $X_{\max}$ was chosen equal to 3.5×10^5. $X_{\max}$ should be very large owing to the use of viscous length scale which is very small ($x = x^*/(\nu_f/U_\infty)$). In addition, $X_{\max}$ should be large in order to get to the far downstream boundary region where we expect Blasius flow to be valid. For such a flow problem, large gradients in flow quantities occur near the wall in the wall normal direction, and near the leading edge in the streamwise direction. For this reason it is necessary to condense more grid points at these locations. To do this, the original uniform grid is transformed to another grid in which the grid points are clustered near the wall and near the leading edge. The transformation used is the Robert's stretching transformation (Anderson *et al.*, 1984). For this problem, there are four boundaries at which boundary conditions have to be specified. Two of these are the wall and freestream. The other two boundaries are the outflow boundaries on the upper and lower sides of the body far downstream from the leading edge.

The governing system of equations and boundary conditions have been discretized using a second order accurate (i.e. $O(\Delta\zeta^2)$, $O(\Delta\eta^2)$) finite difference scheme on a non-uniform grid as follows.

- Interior points: all derivatives in ζ and η have been centrally finite differenced.
- The upper and lower outflow boundaries: all derivatives in η have been centrally finite differenced. All derivatives in ζ have been forward (at the lower outflow boundary) or backward (at the upper outflow boundary) finite differenced, as applied. Also the elliptic terms are neglected.

- The wall and freestream boundaries: all derivatives in ζ have been centrally finite differenced. All derivatives in η have been forward (at the wall) or backward (at freestream) finite differenced, as applied.

Results and discussion

Solution independency

Extensive numerical test calculations were carried out to evaluate the effect of grid size (i.e. number of grid points) on the obtained solution. Attention was focused on the wall vorticity to judge the solution sensitivity. It is found that the solution is more sensitive to the total number of grid points in the wall normal direction (J_{max}) than in the streamwise direction (I_{max}). Almost identical results were obtained for the cases with $I_{max} > 100$ and $J_{max} > 39$. Thus, a grid size of 120×49 was used throughout this study.

Pressure distribution

Using the pressure at downstream infinity as a boundary condition, the surface pressure can be found by integrating from downstream infinity back along the surface.

Equation (27) was integrated using the trapezoidal rule. Figure 2 shows the pressure distribution along the surface for different parabolas in a non-porous medium as a special case. The results are in excellent agreement with those of Haddad *et al.* (2000). Figure 3 shows the effect of the porous medium on the pressure distributions for the case $Da = 2 \times 10^7$, $\Lambda = 0.4$. It can be noted that the porous medium decreases the local pressure. Physically, this is due to the frictional drag and the form drag effect. The microscopic viscous shear stress term (Darcy term) will produce the frictional drag and the microscopic inertial force term will produce the form drag. The effect of Darcy number on the pressure distribution is shown in Figure 4. The pressure decreases as the Darcy number decreases, this is because smaller values of Darcy number lead to larger bulk frictional resistance to the flow in the porous substrate.

The effect of the inertia parameter on the pressure distribution is illustrated in Figure 5. As expected, the local pressure decreases as the inertia parameter increases owing to the increase in the form drag. Note that the effect of Darcy number is more significant on pressure distribution than the inertia parameter effect, especially at low Reynolds number. However, at high Reynolds number, the effect of the microscopic inertia term is more significant since this effect is proportional to u^2 while the microscopic Darcy term is proportional to u.

Figure 6 shows the effect of Viscosity Ratio (VR) on the pressure distribution. As the viscosity ratio increases the frictional drag increases. It is worth mentioning here that the exact value of the viscosity ratio is not settled yet in the literature. An extensive research is carried out to specify the value of this ratio.

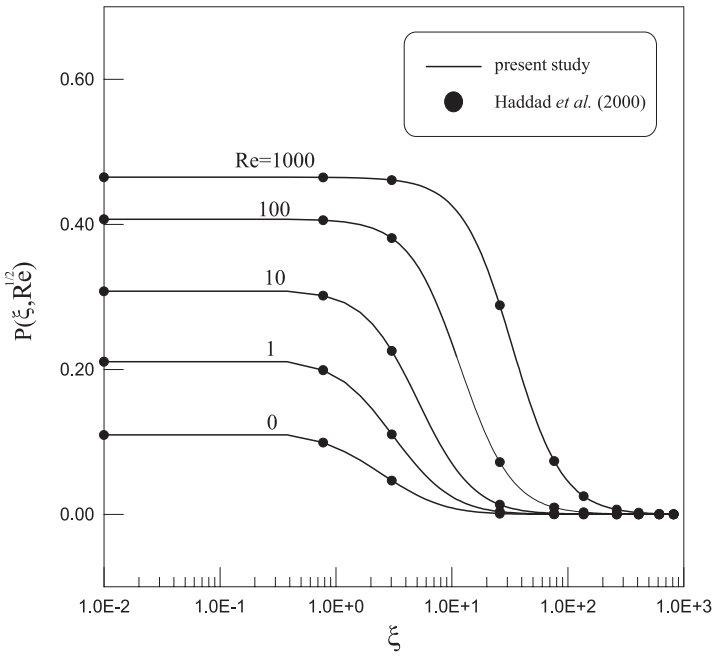

Figure 2.
Surface pressure distribution: $\Lambda = 0.0$ (clear domain)

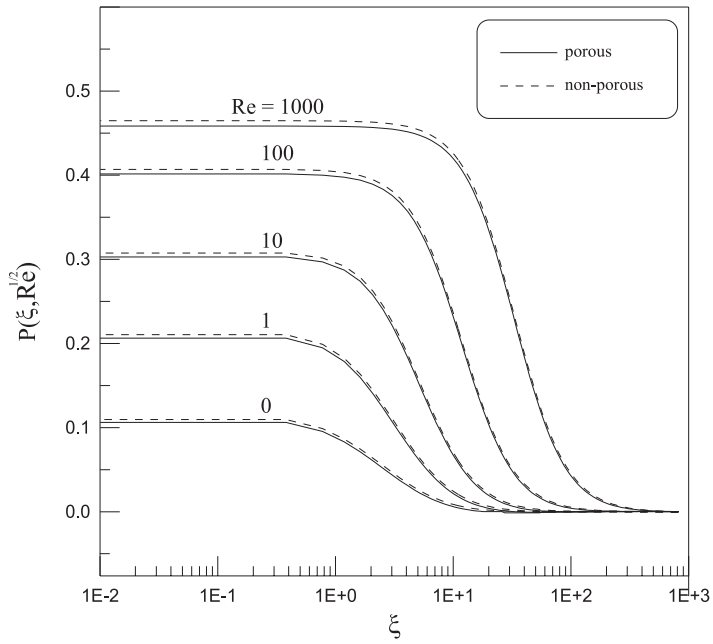

Figure 3.
Surface pressure distribution: $Da = 2 \times 10^7$, $\Lambda = 0.4$ (Porous domain), VR = 1

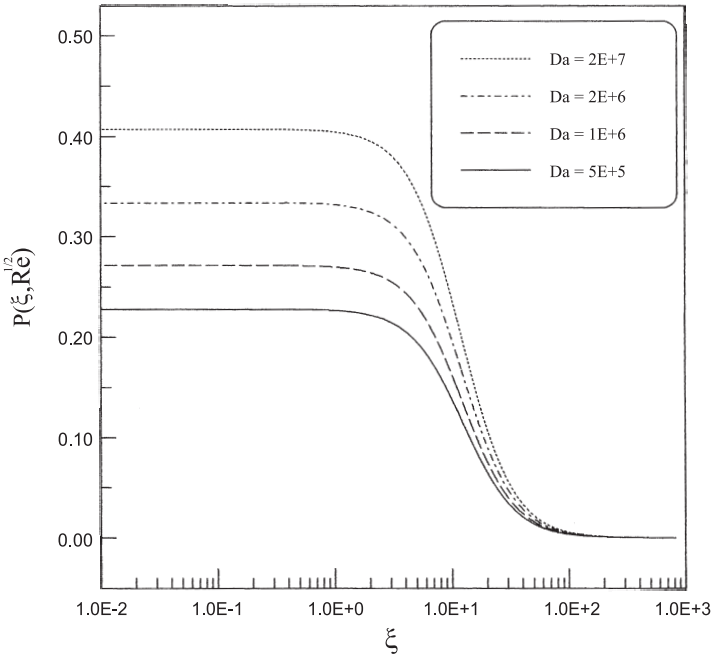

Figure 4.
The effect of Darcy number on surface pressure distribution: $\Lambda = 0.4$, Re = 100, VR = 1

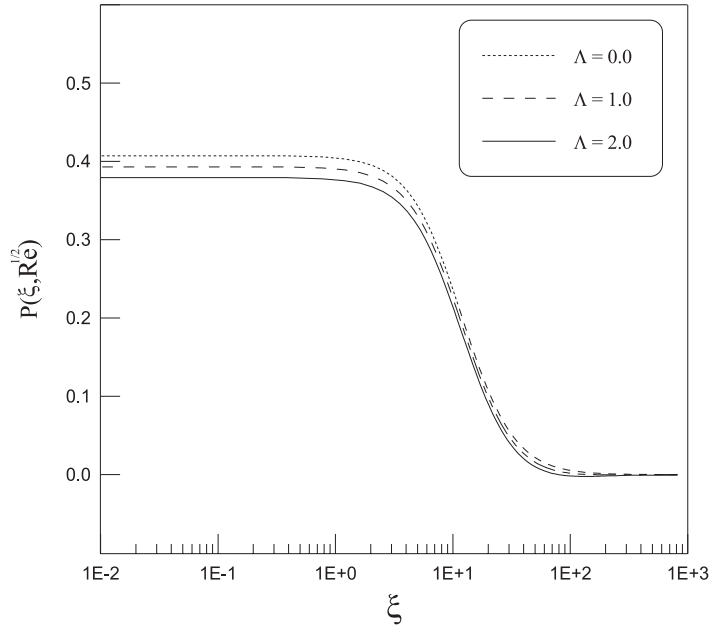

Figure 5.
The effect of inertia parameter on surface pressure distribution: $Da = 2 \times 10^7$, Re = 100, VR = 1

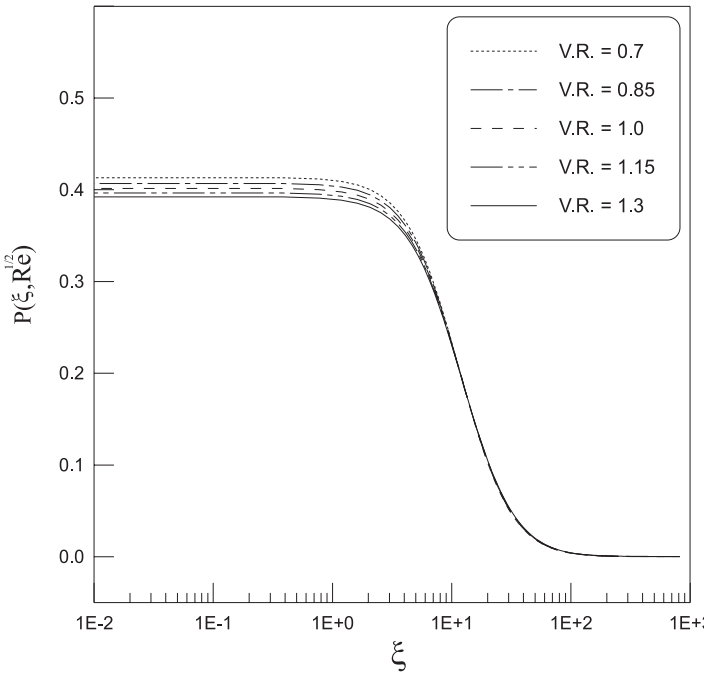

Figure 6.
The effect of viscosity ratio (VR) on surface pressure distribution: $Da = 2 \times 10^7$, $\Lambda = 0.4$, Re = 100

Skin friction distribution

The skin friction distribution for different parabolas in a clear domain is shown in Figure 7. It can be noted that the result obtained agrees very well with those obtained by Haddad *et al.* (2000). The effect of the porous medium on skin friction distribution is similar to that on pressure distribution, as shown in Figure 8. The effect of Darcy number on skin friction distribution is illustrated in Figure 9. As expected the local skin friction coefficient at the wall decreases as the Darcy number decreases. This in turn causes a lower velocity gradient at the wall. To show clearly the effect of the inertia parameter (Λ) on skin friction, a sample result taken from Figure 8 is redrawn for different values of Λ. This is shown in Figure 10. As expected the skin friction decreases as the inertia parameter increases. This is due to the increase in the form drag at the wall. The effect of the viscosity ratio on skin friction distribution is shown in Figure 11. Note that the effect of the viscosity ratio is more significant on skin friction distribution than on the pressure distribution.

Velocity distribution

Figure 12 shows the velocity profile far downstream from the leading edge ($i = 110$) for the case Re = 0 (flat plate), $Da = 2 \times 10^7$, $\Lambda = 0.4$. It can be seen that

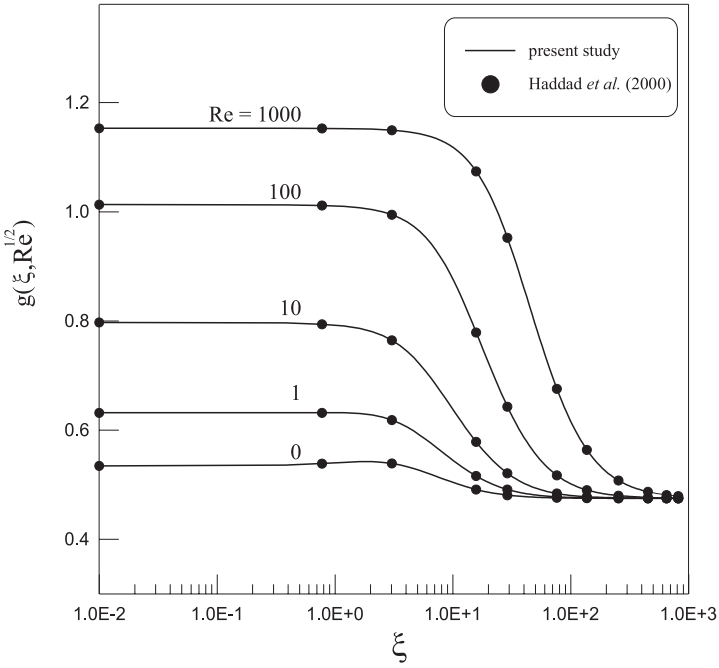

Figure 7.
Skin friction distribution: $\Lambda = 0.0$ (clear domain)

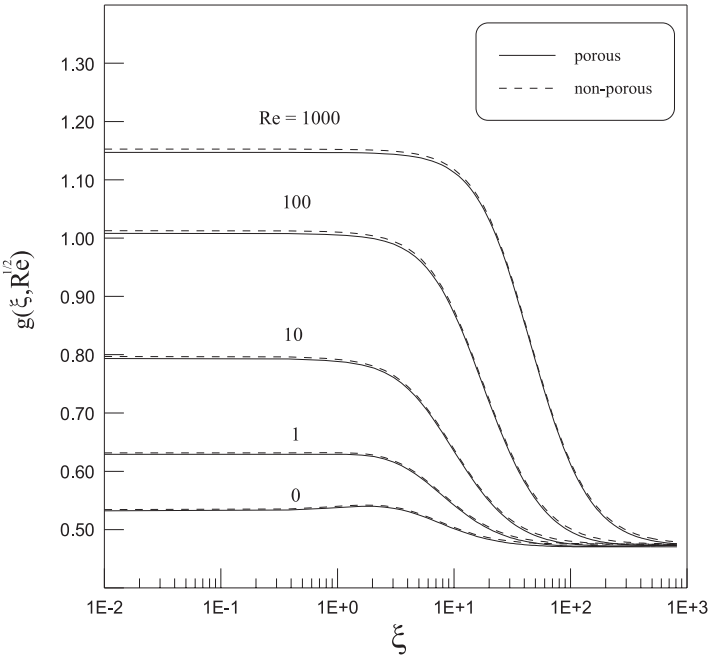

Figure 8.
Skin friction distribution: $Da = 2 \times 10^7$, $\Lambda = 0.4$ (porous domain), VR = 1

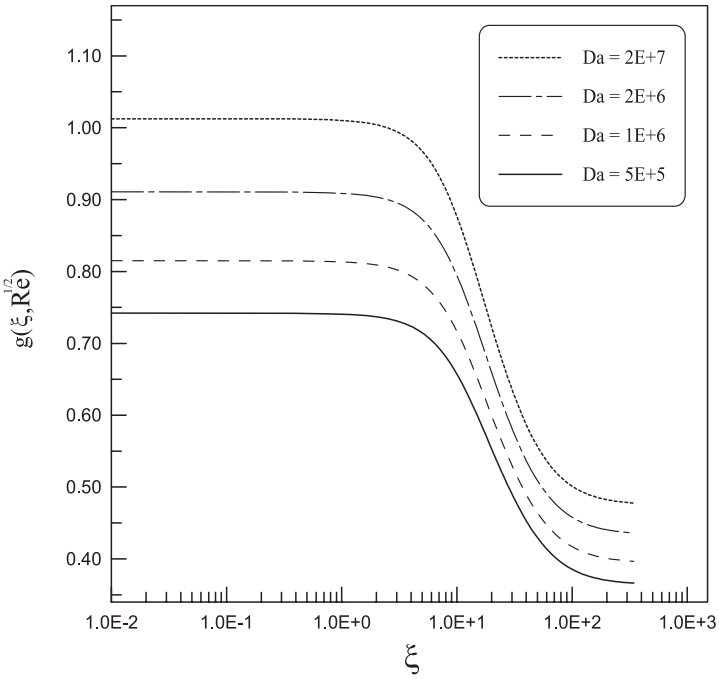

Figure 9.
The effect of Darcy number on skin friction distribution: $\Lambda = 0.4$, Re = 100, VR = 1

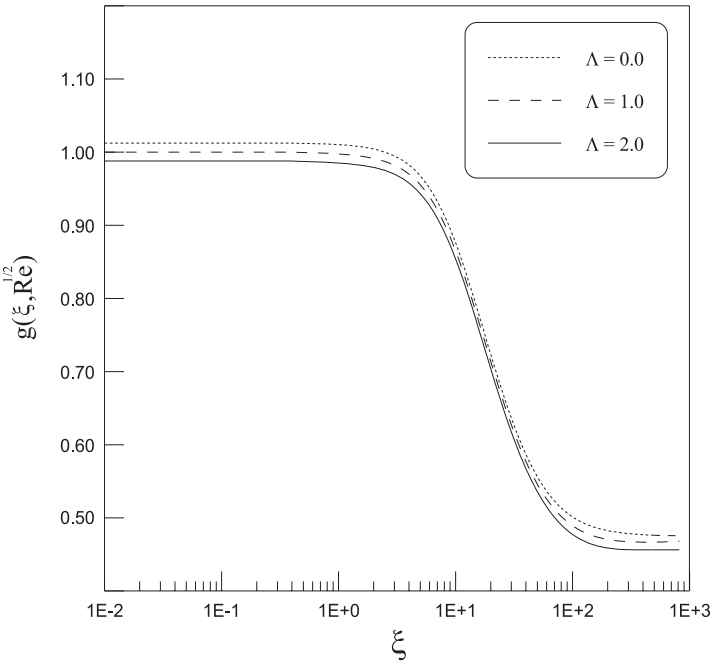

Figure 10.
The effect of inertia parameter on skin friction distribution: $Da = 2 \times 10^7$, Re = 100, VR = 1

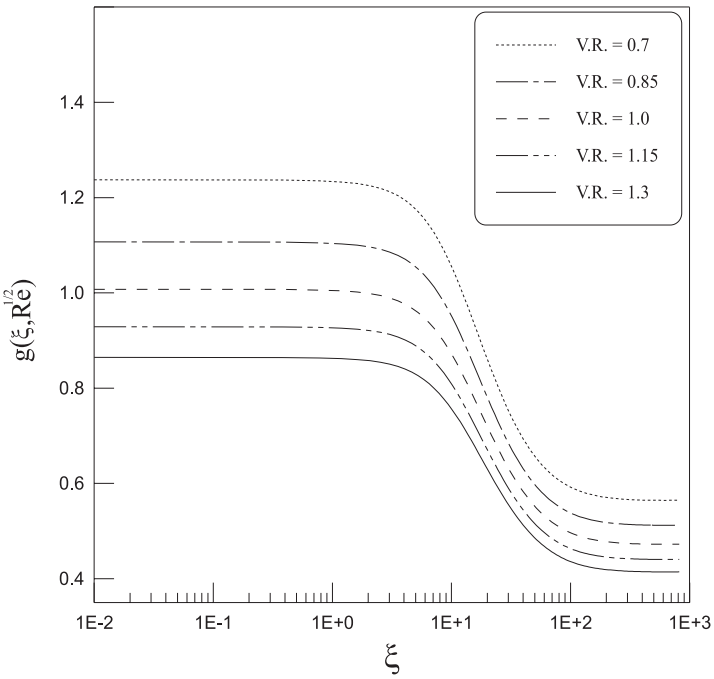

Figure 11.
The effect of viscosity ratio (VR) on skin friction distribution: $Da = 2 \times 10^7$, $\Lambda = 0.4$, $Re = 100$

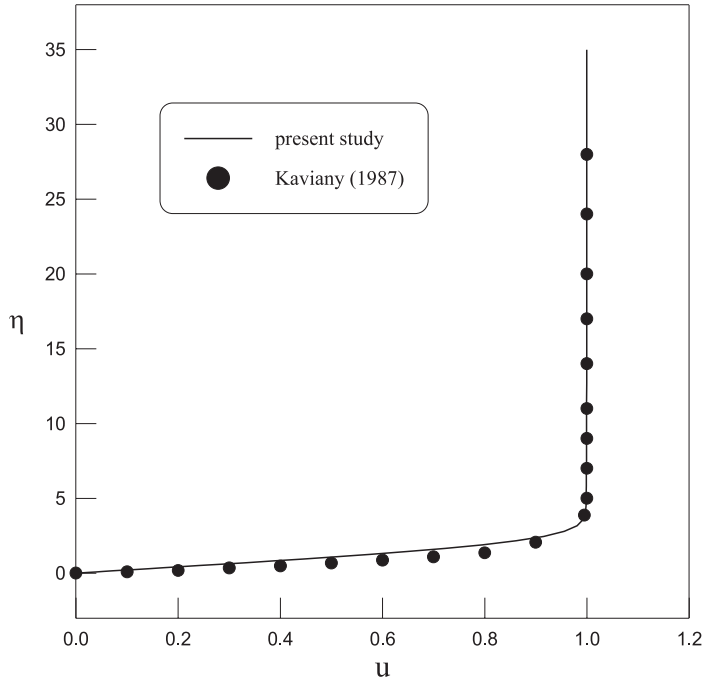

Figure 12.
Local velocity profile: $Re = 0$ (flat plate), $Da = 2 \times 10^7$, $\Lambda = 0.4$

our results are in very good agreement with those of Kaviany (1987). Figure 13 shows the effect of Darcy number on the velocity profile close and away from the leading edge (at i = 10 and 110). It can be noted that as Darcy number decreases the velocity decreases, this is because the bulk frictional resistance to the flow increases as the Darcy number decreases.

Similarly, Figure 14 shows the effect of the inertia parameter on the velocity profile close and away from the leading edge. The decrease in the velocity profile, due to the form drag resistance to the flow, increases as the inertia parameter increases. It should be noted that the Darcy number has the greater effect than the inertia parameter on the velocity profile. This is because the frictional drag effect is bigger than the form drag effect.

Temperature distribution

The temperature profiles in the wall normal direction on a flat plate (Re = 0) away from the leading edge for different values of Prandtl number are shown in Figure 15. To check the thermal part of our solution, the corresponding profiles presented by Schlichting (1979) are drawn in the same figure. Figure 16 shows the temperature profile away from the leading edge (i = 100) for the case Re = 0 (flat plate) and Pr = 0.7 (air). To check our results we compare this

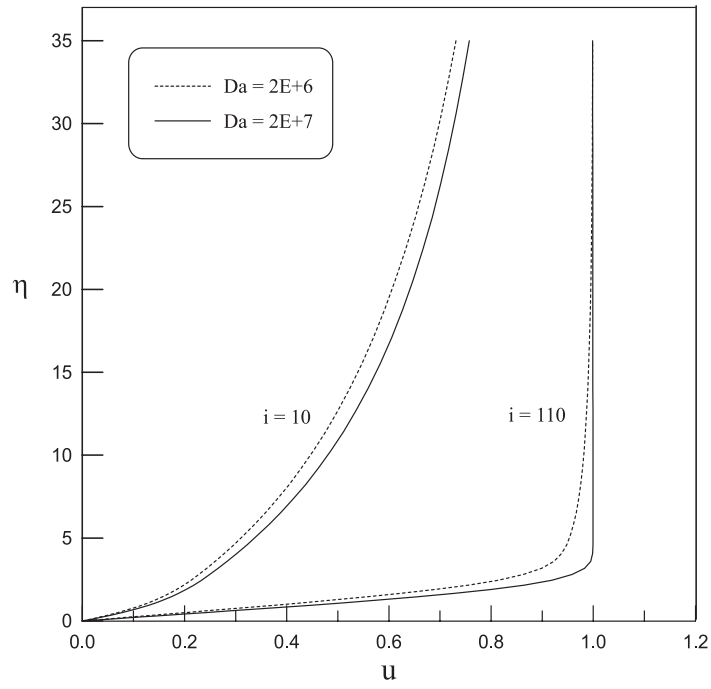

Figure 13.
The effect of Darcy number on local velocity distribution: Λ = 0.4, Re = 100, VR = 1

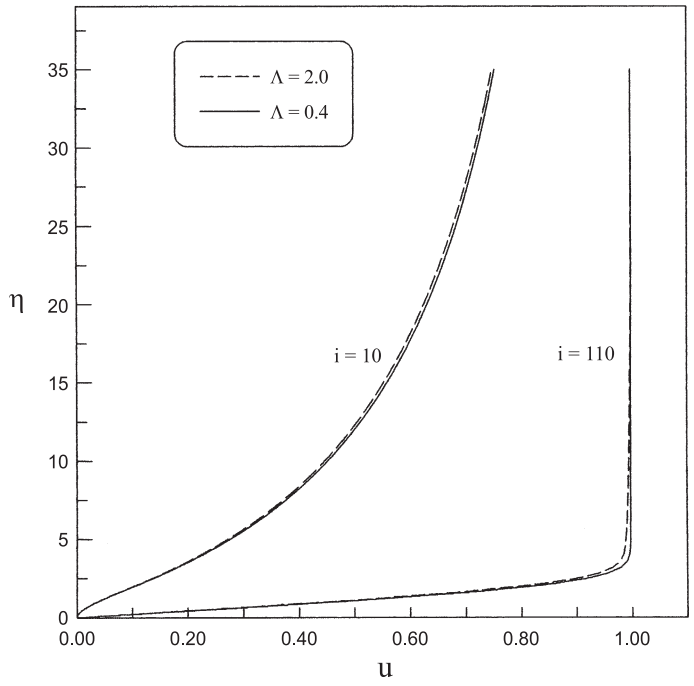

Figure 14.
The effect of inertia parameter (Λ) on local velocity distribution: $Da = 2 \times 10^7$, Re = 100, VR = 1

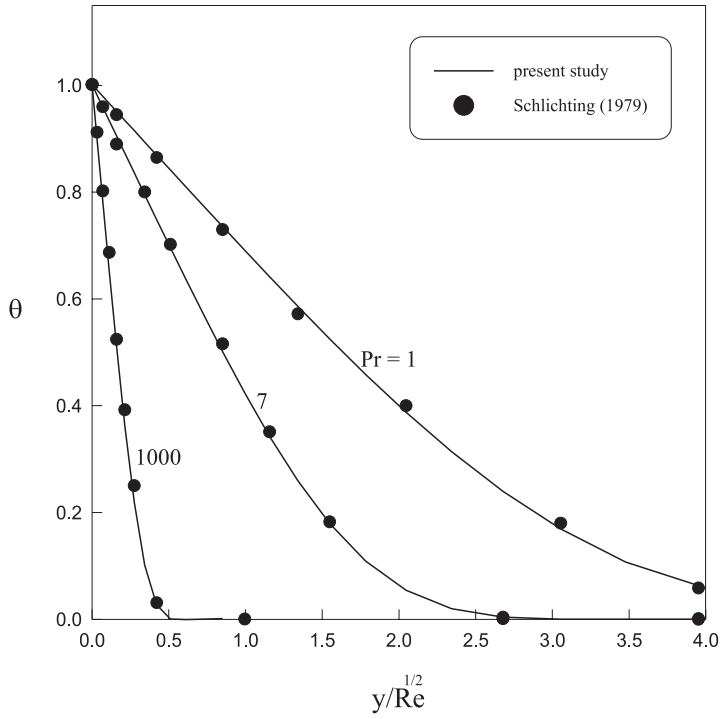

Figure 15.
Temperature profiles: Re = 0 (flat plate)

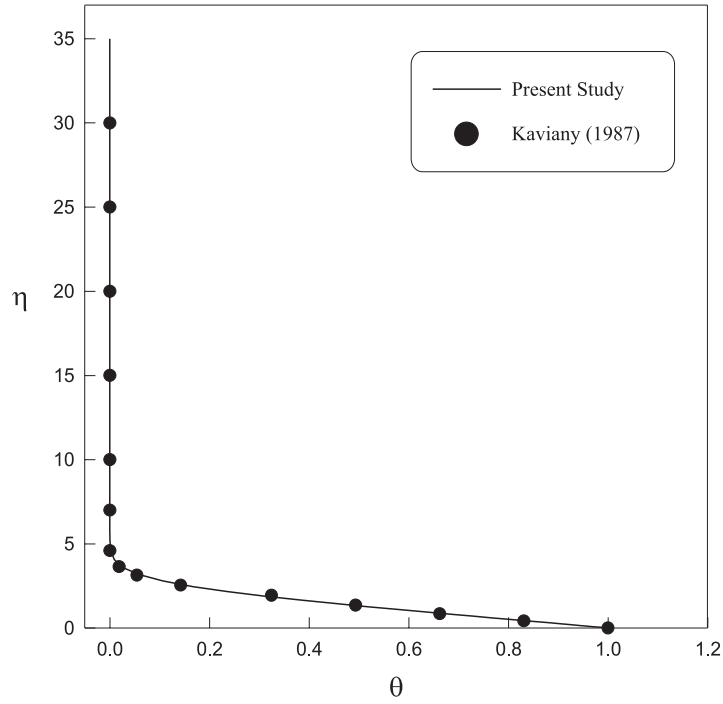

Figure 16.
Temperature profile vs Kaviany result: Pr = 0.7, Re = 0, VR = 1, $Da = 2 \times 10^{7}$, $\Lambda = 0.4$

temperature profile with the one presented by Kaviany (1987). The two profiles agree very well.

Nusselt number distribution

The Prandtl number effect. The Prandtl number effect on the Nusselt number is shown in Figure 17 for the case Re = 100 (parabolic surface). In this figure, the Nusselt number distribution along the surface is shown for a wide range of Prandtl number. As expected, the Nusselt number increases with the increase in Prandtl number. This is because the thermal boundary layer thickness decreases and this in turn enhances the heat transfer. It should be noted that, there is a peak in the curves before they start to asymptote downstream, this might be related to the fact that at the leading edge the flow is a localized accelerating stagnation point flow (Hiemenz flow). This is expected to enhance the mixing action locally and thus, leads to higher Nusselt number.

The Darcy number effect. The effect of Darcy number on the Nusselt number distribution is depicted in Figure 18 for k_r = 1. The Nusselt number decreases as the Darcy number decreases. This is because the presence of the porous substrate and smaller value of Darcy number translate into smaller velocities near the impermeable boundary, which in turn diminish the transfer of the

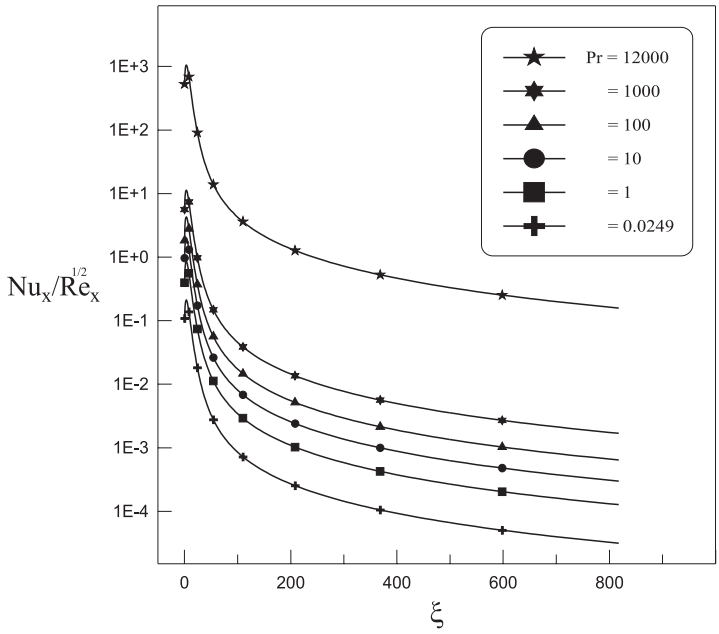

Figure 17.
Effect of Prandtl number on Nusselt number distribution: Re = 100 (parabolic surface), $Da = 2 \times 10^7$, $\Lambda = 0.4$, VR = 1

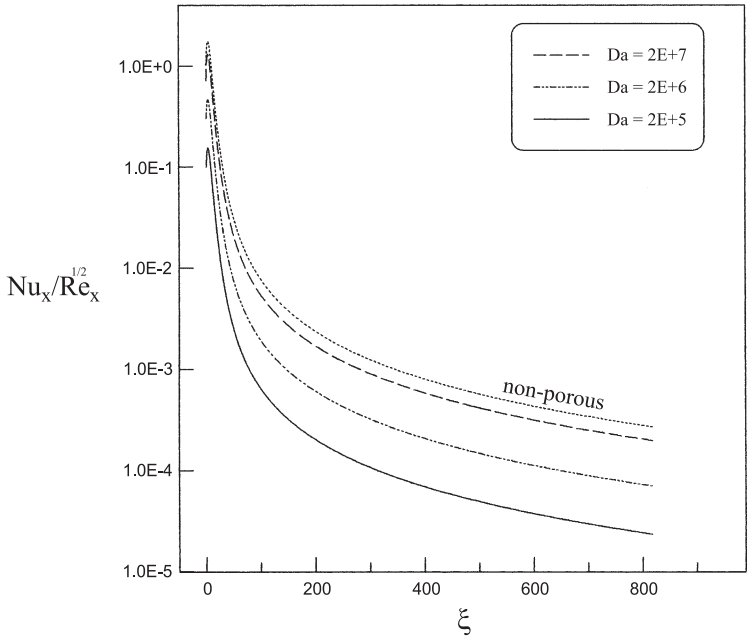

Figure 18.
Effect of Darcy number on Nusselt number distribution: Pr = 1, $\Lambda = 0.4$, Re = 100 (parabolic surface), VR = 1

convective energy. However, it is predicted that Nusselt number will increase due to the increase in the effective thermal conductivity of the domain (for $k_r \gg 1$).

The inertia parameter effect. The effect of inertia parameter on the Nusselt number distribution is depicted in Figure 19. The larger the inertia parameter, the larger will be the bulk form drag that the flow will experience. Therefore, larger values of Λ would result in larger blowing effect through the porous substrate, which would consequently create thicker boundary layer thickness as well as a reduction in the friction coefficient and Nusselt number values.

Effect of the conductivity ratio. The effect of thermal conductivity ratio on Nusselt number distribution is shown in Figure 20, for the case of Prandtl number, Pr = 1, $Da = 2 \times 10^7$ and $\Lambda = 0.4$. As expected, an increase in the conductivity ratio, k_e/k_f, results in an increase in the Nusselt number. This is due to the enhancement in the conduction of heat from the wall to the fluid.

Conclusions

The results of this study point out a number of conclusions, which can be summarized as follows.

(1) There is an excellent agreement between our results and those available in the literature for both hydrodynamic and thermal parts of the problem. This was obviously seen in the pressure, skin friction, velocity and temperature distributions.

(2) Both pressure and skin friction decrease as Darcy number decreases.

(3) Both pressure and skin friction decrease as the inertia parameter increases. Consequently the mass flow rate through the porous substrate decreases. The porous substrate then creates thicker boundary layer and leads to a reduced skin friction coefficient.

(4) As Darcy number decreases and the inertia parameter increases, the velocity profile developed into Blasius profile farther away from the leading edge. Hence, the velocity profile normal to the wall in the clear domain case develops into Blasius profile faster than that in the porous domain case.

(5) It has been shown that the porous substrate significantly reduces the Nusselt number, and the main parameter in reducing the Nusselt number was the Darcy number. On the other hand, the average Nusselt number increases as Prandtl number increases.

(6) It is important to note that one can achieve high Nusselt number values with the presence of a porous substrate. The determining parameter of increasing or decreasing the Nusselt number is the conductivity ratio k_e/k_f.

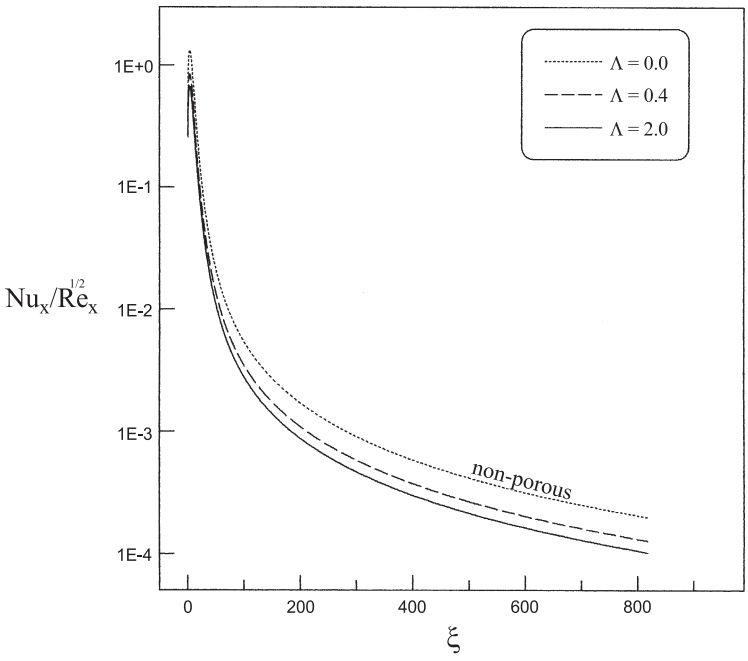

Figure 19.
Effect of inertia parameter on Nusselt number distribution: Pr = 1, Da = 2×10^7, Re = 100 (parabolic surface), VR = 1

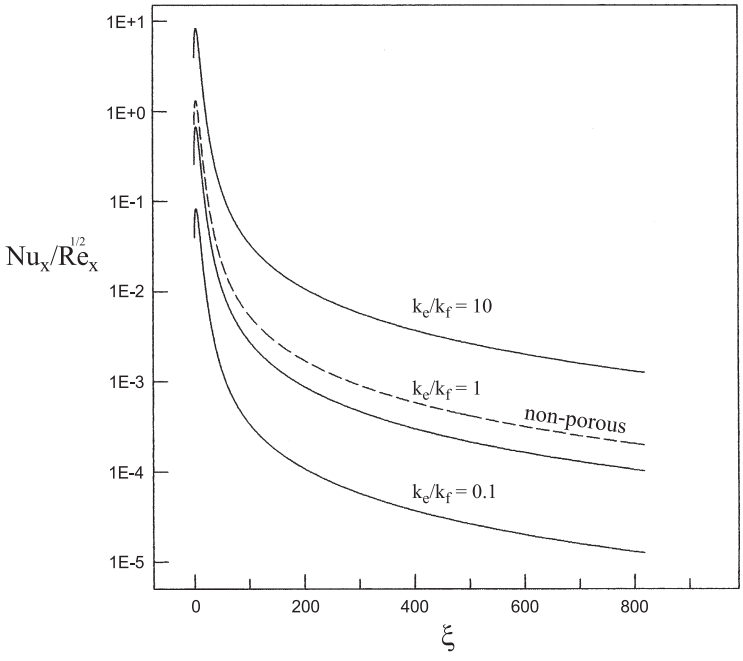

Figure 20.
Effect of the conductivity ratio on Nusselt number distribution: Pr = 1, Da = 2×10^7, Λ = 0.4, Re = 100 (parabolic surface), VR = 1

References

Anderson, D.A., Tannehill, J.C. and Pletcher, R.H. (1984), *Computational Fluid Mechanics and Heat Transfer*, Hemisphere Publishing Corp.

Davis, R.T. (1972), "Numerical solution of the Navier–Stokes equations for laminar incompressible flow past a parabola", *J. Fluid Mech.*, Vol. 51 No. 3, pp. 691–704.

Dennis, S.C.R. and Walsh, J.D. (1971), "Numerical solutions for steady viscous flow past a parabolic cylinder in a uniform stream", *J. Fluid Mech.*, Vol. 50, pp. 801–14.

Dongarra, J.J., Moler, C.B., Bunch, J.R. and Stewart, G.W. (1979), LINPACK User's guide, siam

Haddad, O. and Corke, T. (1998), "Boundary layer receptivity to free-stream sound on parabolic bodies", *J. Fluid Mech.*, Vol. 368, pp. 1–26.

Haddad, O., Abu-Qudais, M. and Maqableh, A. (2000), "Numerical solution of the Navier–Stokes and energy equations for laminar incompressible flow past parabolic bodies", *Int'l J. Numerical Methods for Heat & Fluid Flow*, Vol. 10 No. 1, pp. 80–93.

Haung, P.C. and Vafai, K. (1994), "Analysis of flow and heat transfer over an external boundary covered with a porous substrate", *Journal of Heat Transfer*, Vol. 116, pp. 768–71.

Kaviany, M. (1987), "Boundary-layer treatment of forced convection heat transfer from a semi-infinite flat plate embedded in porous media", *ASME Journal of Heat Transfer*, Vol. 109, pp. 345–9.

Kaviany, M. (1995), *Principles of Heat Transfer in Porous Media*, 2nd ed., Springer, New York, NY.

Lundgern, T.S. (1972), "Slow flow through stationary random beds and suspension of spheres", *J. Fluid Mech.*, Vol. 51, pp. 273–99.

Neale, G. and Nader, W. (1974), "Practical significance of Brinkman's Extension of Darcy's Law: coupled parallel flows within a channel and a boundary porous medium", *Canadian Journal of Chemical Engineering*, Vol. 52, pp. 475–8.

Schlichting, H. (1979), *Boundary Layer Theory*. 7th ed., translated by J. Kestin, McGraw-Hill.

Vafai, K. (1984), "Convective flow and heat transfer in variable porosity media", *J. Fluid Mech.*, Vol. 147, pp. 233–59.

Vafai, K. and Kim, S.J. (1990), "Analysis of surface enhancement by a porous substrate", *Journal of Heat Transfer*, Vol. 112, pp. 700–05.

Vafai, K. and Tien, C.L. (1981), "Boundary and inertia effect on flow and heat transfer in porous media", *Int. J. Heat Mass Transfer*, Vol. 24, pp. 195–203.

Van Dyke, M.D. (1962), "Higher approximations in boundary-layer theory Part 1: general analysis", *J. Fluid Mech.*, Vol. 14, pp. 161–77.